Available online at www.sciencedirect.com
SCIENCE DIRECT®
Image and Vision Computing 23 (2005) 577–586
image AND vision COMPUTING
www.elsevier.com/locate/imavis

Numerical experiments on the accuracy of rotation moments invariants

S. Rodtook*, S.S. Makhanov

Information Technology Program, Sirindhorn International Institute of Technology, Thammasat University, Rangsit Campus, Pathumthani 12121, Thailand

Received 30 January 2004; received in revised form 30 December 2004; accepted 2 February 2005

Abstract

Rotationally invariant moments constitute important techniques applicable to a versatile number of pattern recognition applications. Although the moments are invariant with regard to spatial transformations, in practice, due to the finite screen resolution, the spatial transformation themselves affect the invariance. This phenomenon jeopardizes the quality of pattern recognition. Therefore, this paper presents an experimental analysis of the accuracy and efficiency of discrimination under the impact of the most important spatial transformations such as rotation and scaling. We evaluate experimentally the impact of the noise induced by the spatial transformations on the most popular basis functions such as Zernike polynomials, Mellin polynomials and wavelets. The analysis reveals that the wavelet based moment invariants constitute one of the best choices to construct noise resistant features.

Keywords: Rotation invariant moments; Wavelets

1. Introduction

It has been very well documented that performance of pattern recognition critically depends on whether the employed features are invariant with respect to spatial transformations. The simplest rotationally invariant feature is the Fourier transform of the boundary curve which is invariant with regard to translation and rotation if the coordinate system is appropriately chosen.

A popular class of the invariant features is based on the moment techniques which are believed to be reliable for complex shapes because they involve not solely the contour pixels but all the pixels constituting the object. The first geometric moment invariants introduced by Hu [1–3] are components of the projection of the image onto the monomial functions. However, a dramatic increase in complexity when increasing the order often makes Hu's moments impractical. Besides, the redundancy of the Hu moments noticed in [3] clearly indicates the need for further research. Shortly after Hu's paper, a variety of invariant moments has been proposed and analyzed. The Fourier-Mellin moments [3,7,8] extend classical geometric moments by combining the circular Fourier transform with the radial Mellin function. The complex moments [3,9–11] have been introduced as another simple and straightforward generalization of the geometric moments to the complex plane. The orthogonal moments include the Legendre moments [2–4], the Zernike moments [3–8,15] as well as the less popular Tchebichef [12] and Krawtchouk moments [13]. Orthogonality guarantees that the contribution of each moment coefficient to the entire image is unique and independent. The obvious motivation of the orthogonal moments is the possibility to exactly recover the object image given the infinite set of the moments. In other words, the orthogonality guarantees consistency of the moment based representation. Finally, Shen [14,15] introduced spline wavelet moments representing the image by multiresolution coefficients. It has been demonstrated that such wavelet moment invariants may ensure a higher classification rate.

Sensitivity of the moment invariants to the image noise has been repeatedly mentioned in the literature (see, for

* Corresponding author. Tel.: +66 2501 350520.
E-mail address: sittisak@siit.tu.ac.th (S. Rodtook).

0262-8856/$ - see front matter © 2005 Elsevier B.V. All rights reserved.
doi:10.1016/j.imavis.2005.02.001

instance [3]). As an interesting consequence, the moments are rotationally invariant only when they are computed from the ideal analog images. Even in the absence of noise induced by physical devices there always exists a noise due to a finite resolution of the image subjected to the spatial transformations. Therefore, in practice the spatial transformations themselves affect the invariance. Clearly, this phenomenon might jeopardize the quality of pattern recognition.

Therefore, this paper analyzes accuracy of the moment invariants under the impact of important spatial transformations, such as rotation and scaling. We show the impact on the accuracy and the range of the errors. Furthermore, we demonstrate that the wavelet moment invariants constitute one of the best choices for high accuracy pattern recognition.

2. Rotationally invariant moments

A general moment M of $f(r,\theta)$ with respect to a moment function $F(r,\theta)$ in the polar coordinate system with the origin at the centroid of the object is defined by

$$M = \int_0^{2\pi}\int_0^1 f(r,\theta)F(r,\theta)r\mathrm{d}r\mathrm{d}\theta.$$

In the context of image processing, $f(r,\theta)$ is the image function (the gray level). The continuous image function can be obtained by the standard bilinear interpolation applied to the discrete image. We assume that $F(r,\theta)=\beta(r)\omega(\theta)$, where $\beta(r)$ denotes a family of radial functions and $\omega(\theta)$ an angular function. Taking $\omega(\theta)\equiv\omega_q(\theta)=e^{iq\theta}$ provides the rotational invariance. Note that if q is a continuous variable, then the integral with regard to θ is nothing else than the circular Fourier transform. Usually (but not necessarily), in the theory of rotationally invariant moments q is an integer [14] called the angular order. The choice of $\beta(r)$ defines the type of the invariant. Consider the most popular choices. The Fourier-Mellin moment $M^F_{p,q}$ is characterized by monomials $\beta(r)=r^p$. The complex moment $M^C_{p,q}$ is a generalization of the geometric moments to the complex plane. In the Cartesian coordinates the moment function is defined by $F_{p,q}(x,y)=(x+iy)^p(x-iy)^q$ whereas in the polar coordinates $F_{p,q}(r,\theta)=r^{p+q}e^{i(p-q)\theta}$. Therefore, the radial and the angular functions in this case are given by $\beta(r)=r^{p+q}$, $\omega(\theta)=e^{i(p-q)\theta}$. In order to reduce redundancy the complex moments are defined only for $p\geq q$.

The Zernike moment $M^Z_{p,q}$ is characterized by

$$\beta(r)\equiv Z_{p,q}(r)=\frac{p+1}{\pi}\sum_{s=0}^{(p-|q|)/2}\frac{(-1)^s(p-s)!}{s!\left(\frac{p+|q|}{2}-s\right)!\left(\frac{p-|q|}{2}-s\right)!}r^{p/2-s},$$

where $p\geq|q|$ and $p-|q|$ is even.

Furthermore, we present the above integral by

$$M=\int_0^1\beta(r)\xi(r)r\mathrm{d}r,\quad\text{where}\quad\xi(r)=\int_0^{2\pi}f(r,\theta)\omega(\theta)\mathrm{d}\theta.$$

From the viewpoint of functional analysis, each object is represented by an infinite and unique set of moments if the family of functions $\beta(r)$ constitutes a basis in the appropriate functional space. However, in practice, we always have a finite set of moments affected by noise.

The wavelet bases have a number of advantages since they could be adapted to the spectrum as well as to the spatial properties of a particular set of objects.

In the case of a wavelet basis the set of the basis functions is given by $\psi_{m,n}(r)=\frac{1}{\sqrt{m}}\psi\left(\frac{r-n}{m}\right)$, where $\psi(r)$ is the mother wavelet, m the dilation parameter (the scale index) and n

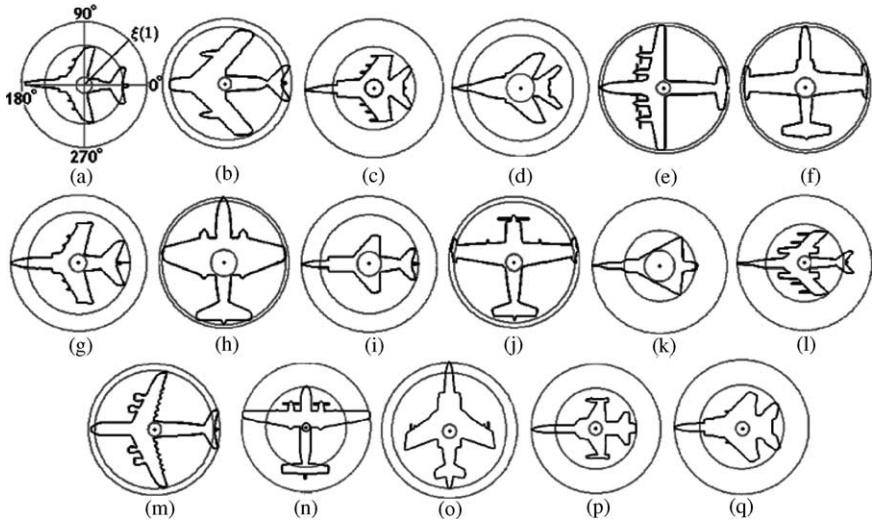

Fig. 1. Seventeen silhouettes of Aircraft (a) Alpha Jet, (b) MiG-17, (c) MiG-25, (d) MiG-29, (e) An-12 Cub, (f) Jastreb, (g) Am-X, (h) Canberra, (i) Yak-36, (j) Brewer, (k) SF-260, (l) Mirage III, (m) Hunter, (n) F-5 Freedom, (o) F-15 Eagle, (p) F-18Hornet, (q) Buccaneer.

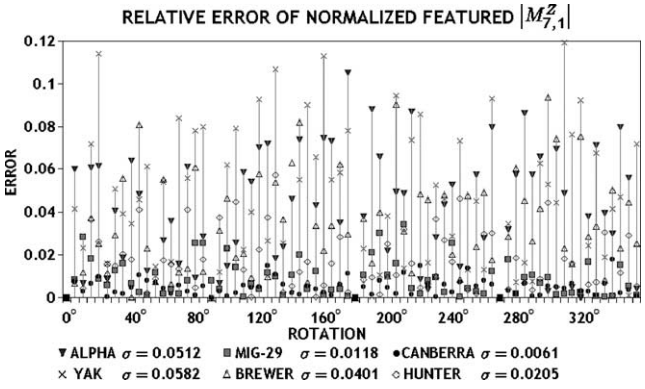

Fig. 2. Impact of rotation.

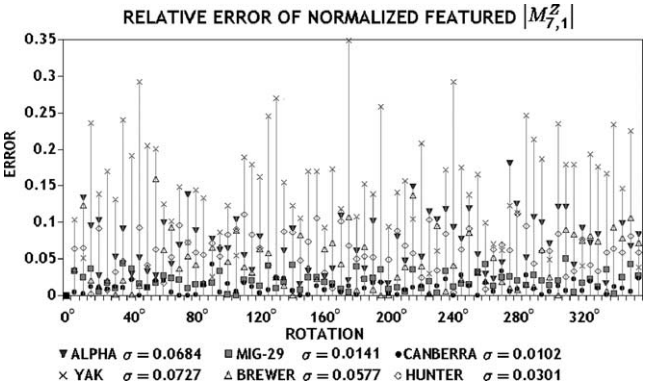

Fig. 3. Impact of scaling and rotation.

the shifting parameter. We denote the wavelet moments by $M^w_{m,n,q}$.

Note that if $\tilde{M}$ is a moment of the rotated image $f(r,\theta+\phi)$, where ϕ is the angle of rotation, then $\tilde{M} = e^{iq\phi}M$. Therefore, $|\tilde{M}| = |M|$. Thus, rotation of the object affects the phase but not the magnitude. Furthermore, $\int_0^1 |\beta(r)|\xi(r)|rdr$ and $\int_0^1 |\beta(r)\xi(r)r|dr$ are rotationally invariant as well.

The moment phase cancellation could be performed by multiplying appropriate powers of moments rather than just by taking the moments magnitudes (since the latter case yields a redundant feature system). Flusser [9,10] has shown that the rotation invariants can be constructed as products $\prod_{i=1}^n M^{k_i}_{p_i,q_i}$ from some minimal set defined by a supplementary integer equation with regard to p_i, q_i and k_i (see [9] for further details). Given the magnitudes, the Flusser's invariants can be evaluated by the identity $\left|\prod_{i=1}^n M^{k_i}_{p_i,q_i}\right| = \prod_{i=1}^n \left|M_{p_i,q_i}\right|^{k_i}$.

3. Experimental set up. Binary images

As mentioned in the introduction, the spatial transformations induce a noise even when physical noise is negligible. It should be noted that, the importance of the effects of the transformational noise is problem-dependent. The decision requires analysis of all the errors involved, such as blurring, illumination, digitization errors, etc. However, there are many cases when the features could be extremely sensitive

Table 1
The standard deviation calculated for the normalized *Fourier-Mellin moment invariants*, Alpha Jet

The standard deviation of Normalized $\|M^F_{p,1}\|$								
$p=1$	$p=2$	$p=3$	$p=4$	$p=5$	$p=6$	$p=7$	$p=8$	$p=9$
0.1967	0.1780	0.1444	0.0742	0.0566	0.0505	0.0490	0.0498	0.0518

Table 2
The standard deviation calculated for the normalized *Zernike moment invariants*, Alpha Jet

The standard deviation of normalized $\|M^Z_{p,1}\|$								
$p=1$	$p=3$	$p=5$	$p=7$	$p=9$	$p=11$	$p=13$	$p=15$	$p=17$
0.0732	0.0245	0.0114	0.0512	0.0073	0.1007	0.0116	0.1208	0.1332

Table 3
The standard deviation calculated for the normalized *wavelet moment invariants*, Alpha Jet (Rotation by using a software (72 images), Physical rotation (80 images))

m	The standard deviation of normalized $\|M^w_{m,n,1}\|$, $(\sigma_1\|\sigma_2)$									
	$n=0$		$n=1$		$n=2$		$n=3$		$n=4$	
	Soft.	Phys.	Soft.	Phys.	Soft.	Phys.	Soft.	Phys.	Soft.	Phys.
0	0.0253	0.0301	0.1019	0.1271	0.0668	0.0820	0.0346	0.0507	0.0282	0.0317
1	0.0057	0.0096	0.0083	0.0173	0.0336	0.0581	0.0287	0.0481	0.0201	0.0417
2	0.0194	0.0317	0.0111	0.0189	0.0251	0.0512	0.0314	0.0549	0.0373	0.0561
3	0.0711	0.0783	0.0655	0.0701	0.0535	0.0692	0.0513	0.0571	0.1264	0.1430

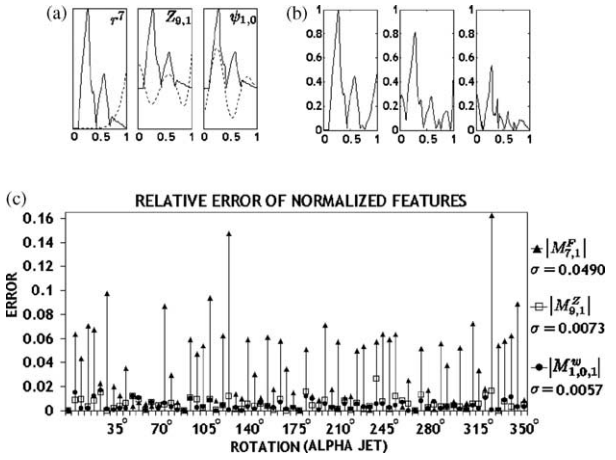

Fig. 4. (a) $\beta(r)$ versus $|\xi_1(r)|$; r^7, $Z_{9,1}$, $\psi_{1,0}$, respectively, (b) $|\beta(r)|-|\xi_1(r)||$ (normalized), (c) The relative error versus the angle.

to the above mentioned transformational noise. For instance, the error induced by the rotation noise for the seventh order Hu's moment applied to the images presented in this chapter is as large as 100%. In this paper we analyze the accuracy of the rotationally invariant moments as applied to aircraft silhouettes in presence of the geometric errors induced by the spatial transforms, namely, by rotation and scaling. We consider silhouettes of seventeen aircraft [17] rotated by 360° with the increment 5° by means of a standard graphics software and by means of physical rotations (see Fig. 1). In order to eliminate accumulation of the error due to multiple re-sampling, each rotation has been performed by rotating the original silhouette corresponding to 0°.

The accuracy is then evaluated by the standard deviation denoted by σ and the relative error denoted by E.

4. Preliminary examples

4.1. Example 1 accuracy of a Zernike moment under the impact of the rotation and scaling

We evaluate the accuracy by measuring the relative error and the standard deviation of the normalized features. Consider the Zernike moments which are among the most popular employed in pattern recognition. Consider $M^Z_{7,1}$, which has the best recognition rate among the Zernike invariants of the first angular order applied to the aircraft set. The quality of recognition was evaluated by using the between-to within-class variance ratio [14]. Fig. 2(a) shows a typical impact of the rotations. The error in $|M^Z_{7,1}|$ varies from 0.0 to 11.91% with the maximum produced by the Yak rotated by 310°. Clearly, rotations may have a significant impact even on the best discriminative features.

Furthermore, scaling produces considerable errors as well. In particular, when combined with rotations. We evaluate the combined impact of scaling and rotation by reducing the original image by 25% and rotating with the increment 5°. The impact on the accuracy is exemplified by

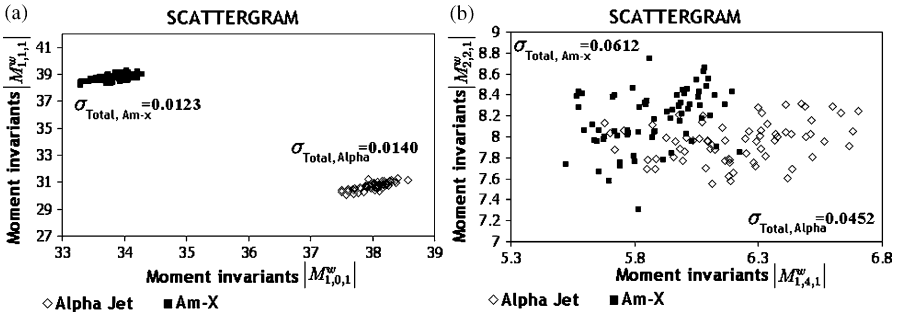

Fig. 5. Scattergram shows the discriminative capabilities of wavelet moment invariants, (a) the pair $(M^w_{1,0,1}, M^w_{1,1,1})$ has high accuracy and produces easily separable sets, (b) the pair $(M^w_{1,4,1}, M^w_{2,2,1})$ has low accuracy and low discrimination.

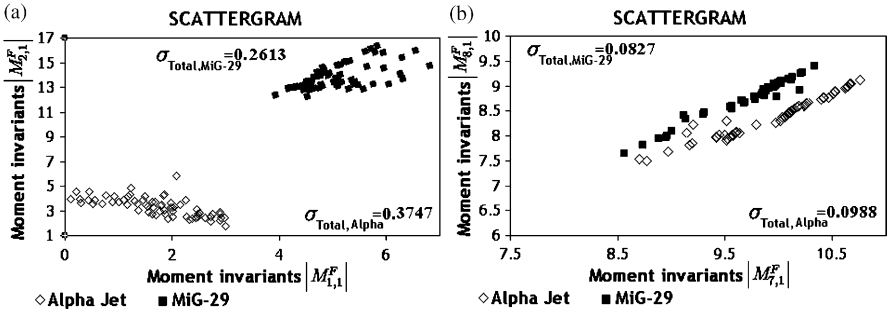

Fig. 6. (a) Pair $(M^F_{1,1}, M^F_{2,1})$ has a low accuracy but a good discrimination rate, (b) pair $(M^F_{7,1}, M^F_{8,1})$ has good accuracy but low discrimination capabilities.

Table 4
The best moment invariants for the aircraft silhouettes

Aircrafts	Moments	Angular order q																	
		$q=1$			$q=2$			$q=3$			$q=4$			$q=5$			$q=6$		
		Best	σ	E	Best	σ	E	Best	σ	E	Best	σ	E	Best	σ	E	Best	σ	E
Alpha Jet	Fourier	(7,1)	0.0490	0.0380	(2,2)	0.0109	0.0091	(4,3)	0.0360	0.0306	(1,4)	0.0039	0.0035	(4,5)	0.0301	0.0264	(1,6)	0.0184	0.0138
	Zernike	(9,1)	0.0073	0.0055	(14,2)	0.0107	0.0087	(7,3)	0.0158	0.0135	(6,4)	0.0042	0.0036	(9,5)	0.0226	0.0170	(20,6)	0.0158	0.0119
	wavelet	(1,0,1)	0.0057	0.0045	(1,2,2)	0.0081	0.0061	(2,1,3)	0.0128	0.0114	(0,0,4)	0.0036	0.0031	(2,2,5)	0.0094	0.0090	(2,2,6)	0.0141	0.0114
MIG-17	Fourier	(4,1)	0.0244	0.0346	(1,2)	0.0308	0.0282	(2,3)	0.0411	0.0387	(1,4)	0.0052	0.0079	(1,5)	0.0098	0.0080	(1,6)	0.0079	0.0090
	Zernike	(7,1)	0.0077	0.0062	(10,2)	0.0105	0.0086	(7,3)	0.0076	0.0092	(6,4)	0.0046	0.0066	(7,5)	0.0097	0.0078	(8,6)	0.0082	0.0093
	Wavelet	(1,2,1)	0.0074	0.0054	(1,0,2)	0.0061	0.0051	(1,2,3)	0.0104	0.0123	(0,0,4)	0.0039	0.0057	(1,2,5)	0.0068	0.0056	(1,2,6)	0.0075	0.0061
MiG-25	Fourier	(4,1)	0.1472	0.0214	(1,2)	0.0127	0.0134	(1,3)	0.0086	0.0120	(1,4)	0.0076	0.0111	(2,5)	0.0206	0.0200	(6,6)	0.0310	0.0290
	Zernike	(3,1)	0.0099	0.0089	(14,2)	0.0086	0.0083	(5,3)	0.0067	0.0079	(6,4)	0.0074	0.0072	(11,5)	0.0180	0.0169	(14,6)	0.0077	0.0062
	Wavelet	(1,2,1)	0.0101	0.0098	(2,3,2)	0.0079	0.0071	(0,0,3)	0.0052	0.0070	(0,0,4)	0.0086	0.0112	(2,2,5)	0.0097	0.0084	(1,0,6)	0.0061	0.0053
MIG-29	Fourier	(4,1)	0.0319	0.0411	(1,2)	0.0104	0.0122	(1,3)	0.0069	0.0095	(1,4)	0.0109	0.0098	(2,5)	0.0158	0.0246	(1,6)	0.0087	0.0074
	Zernike	(7,1)	0.0118	0.0087	(2,2)	0.0084	0.0075	(5,3)	0.0051	0.0043	(14,4)	0.0083	0.0066	(11,5,)	0.0128	0.0137	(8,6)	0.0097	0.0085
	Wavelet	(1,2,1)	0.0117	0.0096	(0,0,2)	0.0101	0.0098	(1,1,3)	0.0047	0.0037	(2,3,4)	0.0094	0.0079	(1,0,5)	0.0127	0.0130	(0,0,6)	0.0074	0.0072
An-12	Fourier	(4,1)	0.0221	0.0215	(2,2)	0.0207	0.0240	(2,3)	0.0096	0.0080	(1,4)	0.0075	0.0080	(1,5)	0.0201	0.0163	(1,6)	0.0158	0.0131
	Zernike	(5,1)	0.0087	0.0079	(10,2)	0.0181	0.0163	(3,3)	0.0076	0.0068	(4,4)	0.0079	0.0084	(7,5)	0.0140	0.0151	(8,6)	0.0191	0.0144
	Wavelet	(0,1,1)	0.0085	0.0070	(1,0,2)	0.0125	0.0107	(0,0,3)	0.0087	0.0079	(0,0,4)	0.0059	0.0053	(0,0,5)	0.0110	0.0103	(0,0,6)	0.0147	0.0129
Jastreb	Fourier	(9,1)	0.0283	0.0655	(1,2)	0.0161	0.0142	(1,3)	0.0068	0.0065	(1,4)	0.0041	0.0021	(1,5)	0.0102	0.0084	(2,6)	0.0204	0.0151
	Zernike	(5,1)	0.0075	0.0061	(12,2)	0.0121	0.0115	(3,3)	0.0075	0.0065	(4,4)	0.0063	0.0043	(5,5)	0.0093	0.0075	(10,6)	0.0103	0.0095
	Wavelet	(1,3,1)	0.0074	0.0061	(1,3,2)	0.0122	0.0141	(0,0,3)	0.0061	0.0056	(0,0,4)	0.0042	0.0021	(0,0,5)	0.0081	0.0062	(1,2,6)	0.0111	0.0097
Am-X	Fourier	(5,1)	0.0327	0.0239	(1,2)	0.0138	0.0110	(2,3)	0.1714	0.0179	(1,4)	0.0040	0.0034	(3,5)	0.0192	0.0161	(2,6)	0.0245	0.0194
	Zernike	(9,1)	0.0082	0.0072	(6,2)	0.0096	0.0068	(7,3)	0.0139	0.0144	(6,4)	0.0034	0.0031	(9,5)	0.0120	0.0104	(12,6)	0.0242	0.0189
	Wavelet	(1,1,1)	0.0059	0.0055	(1,2,2)	0.0114	0.0102	(1,0,3)	0.0140	0.0153	(0,0,4)	0.0027	0.0020	(1,2,5)	0.0083	0.0102	(1,1,6)	0.0218	0.0177
Canberra	Fourier	(1,1)	0.0189	0.0163	(5,2)	0.0512	0.0577	(1,3)	0.0042	0.0033	(1,4)	0.0048	0.0060	(3,5)	0.0118	0.0076	(1,6)	0.0284	0.0354
	Zernike	(7,1)	0.0061	0.0048	(8,2)	0.0110	0.0126	(3,3)	0.0048	0.0039	(4,4)	0.0062	0.0073	(11,5)	0.0097	0.0073	(8,6)	0.0134	0.0105
	Wavelet	(1,1,1)	0.0050	0.0041	(1,1,2)	0.0068	0.0052	(0,0,3)	0.0033	0.0029	(1,2,4)	0.0043	0.0056	(1,1,5)	0.0082	0.0069	(0,0,6)	0.0080	0.0067
Yak-36	Fourier	(6,1)	0.0510	0.0503	(1,2)	0.0079	0.0077	(1,3)	0.0353	0.0298	(1,4)	0.0059	0.0048	(4,5)	0.0385	0.0412	(1,6)	0.0078	0.0072
	Zernike	(9,1)	0.0227	0.0176	(2,2)	0.0070	0.0074	(11,3)	0.0172	0.0181	(6,4)	0.0043	0.0036	(9,5)	0.0126	0.0119	(8,6)	0.0075	0.0066
	Wavelet	(2,4,1)	0.0159	0.0151	(0,0,2)	0.0046	0.0036	(2,2,3)	0.0159	0.0141	(0,0,4)	0.0035	0.0029	(2,3,5)	0.0136	0.0127	(0,0,6)	0.0044	0.0040
Brewser	Fourier	(4,1)	0.0288	0.0246	(4,2)	0.0210	0.0158	(1,3)	0.0070	0.0056	(1,4)	0.0072	0.0064	(1,5)	0.0089	0.0073	(1,6)	0.0211	0.0168
	Zernike	(3,1)	0.0083	0.0091	(14,2)	0.0163	0.0156	(3,3)	0.0079	0.0063	(6,4)	0.0072	0.0063	(5,5)	0.0108	0.0091	(10,6)	0.0093	0.0072
	Wavelet	(1,2,1)	0.0081	0.0078	(2,4,2)	0.0137	0.0124	(0,0,3)	0.0063	0.0051	(0,0,4)	0.0057	0.0049	(0,0,5)	0.0068	0.0054	(1,1,6)	0.0079	0.0066
SF-260	Fourier	(4,1)	0.0203	0.0219	(1,2)	0.0089	0.0081	(1,3)	0.0086	0.0079	(2,4)	0.0189	0.0150	(3,5)	0.0180	0.0176	(1,6)	0.0084	0.0065
	Zernike	(3,1)	0.0082	0.0068	(4,2)	0.0072	0.0078	(5,3)	0.0074	0.0068	(12,4)	0.0168	0.0146	(11,5)	0.0158	0.0141	(8,6)	0.0073	0.0060
	Wavelet	(1,2,1)	0.0095	0.0072	(0,0,2)	0.0068	0.0071	(0,0,3)	0.0073	0.0067	(1,2,4)	0.0147	0.0128	(1,1,5)	0.0146	0.0115	(0,0,6)	0.0058	0.0046
Mirage III	Fourier	(7,1)	0.0311	0.0292	(1,2)	0.0161	0.0130	(1,3)	0.0166	0.0134	(1,4)	0.0098	0.0088	(1,5)	0.0147	0.0157	(1,6)	0.0093	0.0084
	Zernike	(9,1)	0.0122	0.0100	(6,2)	0.0109	0.0093	(11,3)	0.0122	0.0098	(6,4)	0.0074	0.0078	(9,5)	0.0088	0.0073	(8,6)	0.0073	0.0078
	Wavelet	(1,0,1)	0.0078	0.0058	(1,0,2)	0.0104	0.0085	(1,2,3)	0.0110	0.0091	(0,0,4)	0.0071	0.0075	(0,1,5)	0.0080	0.0062	(0,0,6)	0.0064	0.0066
Hunter	Fourier	(4,1)	0.0215	0.0278	(4,2)	0.0184	0.0222	(1,3)	0.0147	0.0184	(1,4)	0.0061	0.0054	(3,5)	0.0184	0.0196	(1,6)	0.0148	0.0164
	Zernike	(11,1)	0.0079	0.0083	(10,2)	0.0175	0.0132	(7,3)	0.0104	0.0078	(6,4)	0.0065	0.0071	(9,5)	0.0133	0.0114	(12,6)	0.0142	0.0151
	Wavelet	(1,1,1)	0.0082	0.0084	(1,0,2)	0.0098	0.0074	(0,1,3)	0.0128	0.0133	(0,0,4)	0.0049	0.0051	(1,1,5)	0.0121	0.0109	(1,5,6)	0.0132	0.0110
F5-Free-dom	Fourier	(5,1)	0.0122	0.0214	(1,2)	0.0211	0.0193	(1,3)	0.0099	0.0084	(2,4)	0.0020	0.0129	(2,5)	0.0207	0.0252	(1,6)	0.0139	0.0131
	Zernike	(7,1)	0.0100	0.0172	(12,2)	0.0197	0.0171	(5,3)	0.0129	0.0119	(6,4)	0.0075	0.0073	(11,5)	0.0176	0.0155	(8,6)	0.0157	0.0142
	Wavelet	(0,1,1)	0.0095	0.0074	(1,1,2)	0.0146	0.0163	(0,0,3)	0.0097	0.0076	(0,1,4)	0.0068	0.0065	(1,2,5)	0.0137	0.0133	(0,0,6)	0.0131	0.0129

(*continued on next page*)

Table 4 (*continued*)

Aircrafts	Moments	Angular order q															
		$q=1$			$q=2$			$q=3$			$q=4$			$q=5$			$q=6$		
		Best	σ	E	Best	σ	E	Best	σ	E	Best	σ	E	Best	σ	E	Best	σ	E
F-15	Fourier	(6,1)	0.0323	0.0154	(2,1)	0.0126	0.0117	(2,3)	0.0181	0.0149	(2,4)	0.0062	0.0055	(2,5)	0.0183	0.0161	(3,6)	0.0395	0.0194
Eagle	Zernike	(9,1)	0.0093	0.0078	(2,2)	0.0014	0.0104	(7,3)	0.0178	0.0136	(8,4)	0.0044	0.0042	(9,5)	0.0112	0.0157	(12,6)	0.0245	0.0188
	Wavelet	(1,1,1)	0.0064	0.0052	(0,1,2)	0.0106	0.0094	(1,0,3)	0.0111	0.0109	(1,0,4)	0.0038	0.0031	(1,0,5)	0.0091	0.0078	(1,1,6)	0.0200	0.0179
F-18 Hornet	Fourier	(8,1)	0.0194	0.0141	(1,2)	0.0160	0.0143	(1,3)	0.0085	0.0071	(1,4)	0.0063	0.0053	(2,5)	0.0157	0.0132	(2,6)	0.0211	0.0176
	Zernike	(11,1)	0.0086	0.0071	(12,2)	0.0151	0.0140	(3,3)	0.0097	0.0075	(6,4)	0.0073	0.0067	(7,5)	0.0121	0.0085	(12,6)	0.0109	0.0099
	Wavelet	(1,1,1)	0.0075	0.0067	(1,1,2)	0.0119	0.0097	(0,0,3)	0.0071	0.0066	(0,0,4)	0.0042	0.0039	(2,1,5)	0.0089	0.0070	(1,0,6)	0.0132	0.0118
Buccaneer	Fourier	(5,1)	0.0209	0.0414	(5,2)	0.0132	0.0098	(1,3)	0.0094	0.0121	(2,4)	0.0132	0.0160	(2,5)	0.0172	0.0201	(1,6)	0.0087	0.0129
	Zernike	(7,1)	0.0125	0.0115	(10,2)	0.0101	0.0091	(3,3)	0.0081	0.0098	(14,4)	0.0107	0.0110	(13,5)	0.0153	0.0150	(8,6)	0.0096	0.0153
	Wavelet	(1,2,1)	0.0120	0.0094	(1,0,2)	0.0083	0.0077	(0,0,3)	0.0054	0.0059	(2,3,4)	0.0085	0.0097	(1,0,5)	0.0115	0.0121	(0,0,6)	0.0081	0.0107

$|M^Z_{7,1}|$ applied to represent six aircraft silhouettes (see Fig. 3). The maximum relative error in $|M^Z_{7,1}|$ is as large as 34.91% for Yak rotated by 175°.

4.2. Example 2 why the wavelet moments perform better

This experiment shows the accuracy of multiresolution moment invariants based on the B-spline wavelets [16]. In this case the mother B-spline wavelet is given by

$$\psi(r)=\frac{4a^{k+1}}{\sqrt{2\pi(k+1)}}\sigma_w\cos(2\pi f_0(2r-1))\exp\left(-\frac{(2r-1)^2}{2\sigma_w^2(k+1)}\right),$$

where $k=3$, $a=0.7$, $f_0=0.41$ and $\sigma_w^2=0.56$. Consider a silhouette of Alfa Jet. Tables 1–3 show the standard deviation corresponding to M^F, M^Z and M^W, respectively. Plots of the most accurate moments of the first angular order for each moment are shown in Fig. 4, namely, $M^F_{7,1}$ (the maximum error is 13.25%), $M^Z_{9,1}$ (2.61%), $M^w_{1,0,1}$ (1.7%). The plots illustrate why the wavelet basis performs better. It is because of the adaptable shape of the wavelet that the maximum of the wavelet basis function almost coincides with maximum of $|\xi(r)|$. It is clear that if $|\xi(r)|$ is large then $|\beta(r)|$ should be large and if $|\xi(r)|$ is small, then $|\beta(r)|$ should be small. In other words, if the $|\beta(r)|$ behaves similarly to $|\xi(r)|$ then it is good for representing $\xi(r)$ in terms of the integral $M=\int_0^1\beta(r)\xi(r)r\mathrm{d}r$ which is nothing else than a dot product in a functional space. Let us evaluate this similarity by calculating the difference $\Delta(r)\equiv||\beta(r)|-|\xi(r)||$. The plots of the normalized $\Delta(r)$ are shown in Fig. 4(b). The smallest $\Delta(r)$ is achieved for M^w due to the good adaptation properties of the wavelet. Clearly, the Zernike polynomials cannot be adapted as close as the wavelets, moreover they oscillate when the order increases. Finally, the Fourier-Mellin moments represented by monomials are not competitive at all. The high order monomials vanish when r is close to 0. Consequently they simply 'wash out' information relevant to $\beta(r)$.

Furthermore, Table 3 displays the comparison of rotations performed physically and by the software. Clearly, the errors are varying in the same magnitude. However, physical rotations followed by capture produce larger errors due to illumination, additional random noise, etc.

4.3. Example 3 accuracy and recognition rate

Consider a combination of the moment invariants affected by rotations. The features shown in Figs. 5 and 6 are calculated for Alfa-Jet, Am-X and MiG-29. Fig. 5 shows the relevance of the accuracy and discriminative capabilities in the case of wavelets. The wavelet features shown in Fig. 5(a) and (b) demonstrate that the high accuracy usually leads to high recognition rate whereas low accuracy moments create hardly separable features. However, it is not always the case for other moments. Fig. 6(a) and (b) show that although a pair of the Fourier-Mellin moments

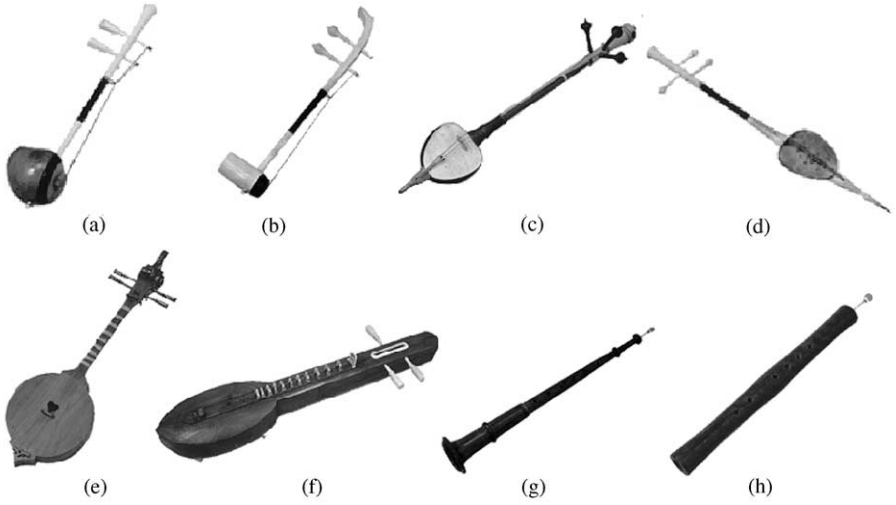

Fig. 7. Grayscale images of Thai musical instruments (a) 'SAW DUANG' (Fiddle), (b) 'SAW OU' (Fiddle), (c) 'SALOR' (Lute), (d) 'SAW SAM SAI' (Fiddle), (e) 'SUENG' (Lute), (f) 'JAKAE' (Lute), (g) 'PEE CHAWA' (Pipe), (h) 'PEE NOKE' (Pipe).

$(M^F_{7,1}, M^F_{8,1})$ displays relatively good accuracy $\sigma_{MiG}=0.0827$, $\sigma_{\text{Alfa}}=0.0988$ discrimination will be better in case of $(M^F_{1,1}, M^F_{2,1})$ characterized by $\sigma_{MiG}=0.2613$, $\sigma_{\text{Alfa}}=0.3747$.

5. Comparison of the moment invariants

We present now a series of experiments performed on the 17 basic aircraft silhouettes. Since different angular orders usually amplify different frequencies of the rotation noise, it is not possible to always find one small set of basis wavelets suitable to represent all the angular orders. Besides the most accurate moment invariants are different for different aircraft types. The accuracy of the wavelet moment invariants has been compared with the Zernike and the Fourier-Mellin moment invariants. Since the performance of the complex moments is very close to that of the Fourier-Mellin moments the complex moments are omitted. Table 4 shows the relative error along with the standard deviation for the best moment for each angular order and for each type. Surprisingly, the wavelet basis is almost uniformly better then the Zernike and the Fourier-Mellin basis. As a matter of fact, M^w overperforms M^Z and M^F in 83% from the 102 experiments. However, certain Zernike functions may be better suited for a particular silhouette such as $M^Z_{2,2}$ for MIG-29, $M^Z_{7,3}$ for MIG-17, $M^Z_{3,3}$ for An-12, etc.

6. Accuracy of the moment invariants applied to grayscale images and remarks on the spectral properties

This chapter introduces an experimental set consisting of eight grayscale images [18] shown in Fig. 7. Since the moment invariants depend now on the overall intensities of the image the transformational noise displays much more profound impact. The objects were selected due to their elongated shape. In this case the effects of rotation are more pronounced. The increase in sensitivity to the noise can also be explained by complicated contours such that the centroid often lies outside the image body. Table 5 shows that for the grayscale images the wavelet based moments are more accurate then the conventional moments.

The moments considered in the frequency domain when the object is subjected to the 'conventional' high frequency noise as well as to the transformational noise exhibit similar behavior. The accuracy of the Fourier transform of $\beta(r)\xi(r)r$ for different $\beta(r)$ shows that in the frequency domain the most accurate wavelet is usually the best as compared to other moments. It exhibits a better recognition rate as well. Moreover, the high accuracy in the time domain usually leads to the high accuracy in the frequency domain and vise versa.

Finally, note that the monomials r^p, r^{p+q} corresponding to the Fourier-Mellin and the complex moment are typical low-pass filters evolving into the band-stop filter as the order

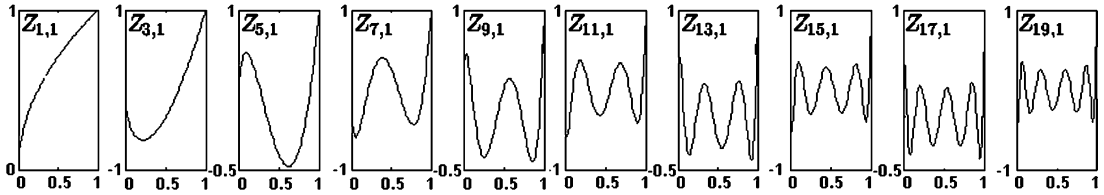

Fig. 8. The Zernike basis functions.

Table 5
The best moment invariants for the grayscale images

Aircrafts	Moments	Angular order q																	
		$q=1$			$q=2$			$q=3$			$q=4$			$q=5$			$q=6$		
		Best	σ	E	Best	σ	E	Best	σ	E	Best	σ	E	Best	σ	E	Best	σ	E
Saw	Fourier	(2,1)	0.0283	0.0227	(1,2)	0.0089	0.0091	(3,3)	0.0267	0.0215	(1,4)	0.0126	0.0095	(3,5)	0.0318	0.0255	(1,6)	0.0186	0.0120
Duang	Zernike	(5,1)	0.0121	0.0097	(4,2)	0.0071	0.0068	(7,3)	0.0171	0.0147	(6,4)	0.0138	0.0099	(9,5)	0.0256	0.0214	(6,6)	0.0217	0.0153
	wavelet	(1,2,1)	0.0086	0.0070	(0,1,2)	0.0070	0.0067	(1,2,3)	0.0106	0.0120	(0,0,4)	0.0108	0.0077	(1,2,5)	0.0169	0.0133	(0,0,6)	0.0149	0.0118
SAW OU	Fourier	(7,1)	0.0289	0.0313	(1,2)	0.0091	0.0103	(2,3)	0.0284	0.0261	(1,4)	0.0083	0.0091	(6,5)	0.0273	0.0310	(1,6)	0.0092	0.0075
	Zernike	(11,1)	0.0206	0.0210	(2,2)	0.0316	0.0178	(11,3)	0.0208	0.0179	(4,4)	0.0089	0.0115	(11,5)	0.0131	0.0145	(6,6)	0.0101	0.0090
	Wavelet	(2,4,1)	0.0124	0.0153	(0,0,2)	0.0086	0.0067	(2,3,3)	0.0152	0.0175	(0,0,4)	0.0077	0.0065	(2,4,5)	0.0126	0.0108	(0,0,6)	0.0088	0.0067
SALOR	Fourier	(4,1)	0.0179	0.0167	(1,2)	0.0098	0.0107	(5,3)	0.0168	0.0141	(6,4)	0.0382	0.0211	(7,5)	0.0167	0.0195	(1,6)	0.0108	0.0159
	Zernike	(3,1)	0.0084	0.0078	(4,2)	0.0076	0.0069	(7,3)	0.0128	0.0095	(14,4)	0.0277	0.0181	(13,5)	0.0164	0.0194	(6,6)	0.0157	0.0188
	Wavelet	(1,2,1)	0.0077	0.0071	(0,1,2)	0.0086	0.0081	(1,1,3)	0.0097	0.0091	(1,1,4)	0.0141	0.0115	(1,0,5)	0.0132	0.0150	(0,1,6)	0.0122	0.0182
SAW	Fourier	(4,1)	0.0391	0.0296	(1,2)	0.0144	0.0204	(4,3)	0.0400	0.0317	(1,4)	0.0157	0.0154	(3,5)	0.0426	0.0366	(1,6)	0.0166	0.0203
SAM SAI	Zernike	(5,1)	0.0095	0.0082	(2,2)	0.0128	0.0116	(7,3)	0.0275	0.0241	(4,4)	0.0176	0.0212	(13,5)	0.0410	0.0326	(6,6)	0.0232	0.0249
	Wavelet	(1,0,1)	0.0127	0.0118	(1,0,2)	0.0111	0.0108	(0,1,3)	0.0195	0.0163	(0,0,4)	0.0157	0.0151	(2,2,5)	0.0214	0.0253	(0,0,6)	0.0159	0.0184
SUENG	Fourier	(3,1)	0.0212	0.0160	(1,2)	0.0132	0.0079	(2,3)	0.0180	0.0129	(1,4)	0.0145	0.0091	(2,5)	0.0204	0.0166	(1,6)	0.0151	0.0097
	Zernike	(7,1)	0.0098	0.0073	(4,2)	0.0101	0.0067	(11,3)	0.0169	0.0098	(4,4)	0.0149	0.0117	(13,5)	0.0166	0.0113	(6,6)	0.0176	0.0112
	Wavelet	(1,0,1)	0.0082	0.0059	(0,0,2)	0.0085	0.0059	(1,2,3)	0.0094	0.0084	(2,0,4)	0.0108	0.0081	(1,1,5)	0.0120	0.0112	(0,0,6)	0.0148	0.0095
JAKAE	Fourier	(3,1)	0.0221	0.0146	(1,2)	0.0132	0.0085	(1,3)	0.0180	0.0168	(1,4)	0.0150	0.0084	(4,5)	0.0261	0.0242	(2,6)	0.0271	0.0228
	Zernike	(3,1)	0.0116	0.0109	(4,2)	0.0091	0.0075	(9,3)	0.0169	0.0127	(6,4)	0.0147	0.0077	(15,5)	0.0192	0.0180	(16,6)	0.0164	0.0138
	Wavelet	(1,0,1)	0.0082	0.0073	(0,0,2)	0.0088	0.0068	(1,1,3)	0.0098	0.0079	(0,0,4)	0.0139	0.0071	(2,1,5)	0.0140	0.0112	(2,1,6)	0.0161	0.0120
PEE	Fourier	(5,1)	0.0401	.0322	(3,2)	0.0139	0.0177	(5,3)	0.0398	0.0319	(1,4)	0.0159	0.0144	(5,5)	0.0387	0.0316	(1,6)	0.0153	0.0181
CHAWA	Zernike	(3,1)	0.0161	0.0139	(6,2)	0.0116	0.0127	(5,3)	0.0211	0.0177	(6,4)	0.0140	0.0129	(7,5)	0.0257	0.0241	(8,6)	0.0185	0.0238
	Wavelet	(1,1,1)	0.0160	0.0135	(1,1,2)	0.0101	0.0121	(1,1,3)	0.0165	0.0132	(0,0,4)	0.0119	0.0099	(1,1,5)	0.0173	0.0134	(0,0,6)	0.0126	0.0113
PEE	Fourier	(7,1)	0.0667	0.0612	(4,2)	0.0109	0.0133	(4,3)	0.0660	0.0609	(1,4)	0.0132	0.0095	(7,5)	0.0821	0.0603	(1,6)	0.0154	0.0143
NOK	Zernike	(5,1)	0.0553	0.0503	(10,2)	0.0079	0.0087	(11,3)	0.0380	0.0498	(6,4)	0.0092	0.0083	(7,5)	0.0656	0.0535	(8,6)	0.0113	0.0092
	Wavelet	(1,3,1)	0.0386	0.0443	(1,3,2)	0.0072	0.0063	(1,3,3)	0.0357	0.0425	(0,0,4)	0.0084	0.0078	(1,3,5)	0.0383	0.0489	(0,0,6)	0.0085	0.0068

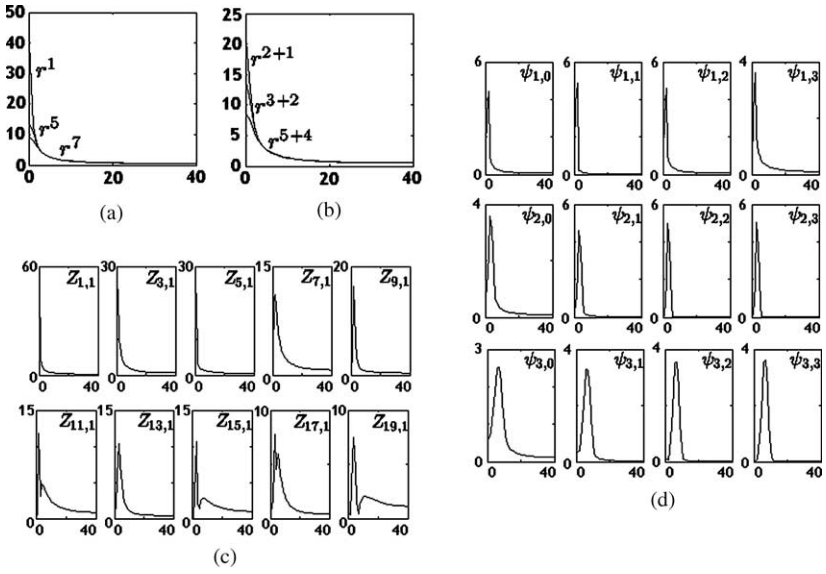

Fig. 9. (a)–(d) Spectrum of the moment radial functions, (a) the Fourier-Mellin basis, (b) the complex basis, (c) the Zernike basis, (d) the B-spline wavelet basis.

increases (Fig. 9(a) and (b)). The Zernike basis functions in the spatial domain (see Fig. 8) are characterized by increasing oscillations. Consequently, in the frequency domain, the Zernike function becomes more and more similar to a band-pass filter (Fig. 9(c)). The higher is the order the more to the right the pass-band moves. However, the resulting filter is not smooth and the pass band is difficult to control. As opposed to the basis functions above, the wavelets make it possible to better control the spectral characteristics. Besides, the wavelet basis function (see Fig. 9(d)) exhibits smooth band-pass characteristics. Fig. 10 shows $\xi(r)$ the frequency domain. Again the wavelet adapts better to the peak at the low frequency and therefore provides better accuracy then the Zernike polynomial. $Z_{5,1}$, $\psi_{1,2}$ correspond to the best Zernike and wavelet, respectively. The error in the low frequency area is 0.942 and 0.802, respectively which exemplifies the advantages of wavelets in the frequency domain as well.

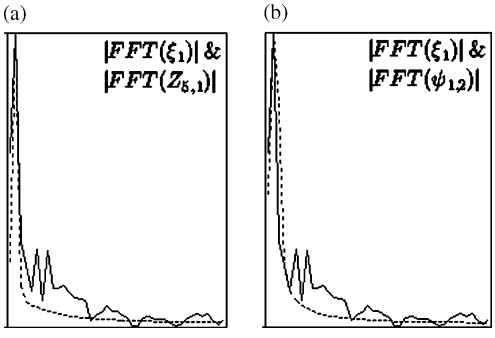

Fig. 10. (a) SAW DUANG and the best Zernike polynomial in the frequency domain, (b) SAW DUANG and the best wavelet in the frequency domain.

7. Conclusion

We analyze the behavior the Zernike, Fourier-Mellin, complex and wavelet moment invariants under the impact of rotation and scaling. Although the moments are invariant with regard to the spatial transformations, in practice the transformation themselves affect the invariance. Noise sensitive invariants such as Hu's moment could be dramatically affected by the noise. Moreover, less sensitive moments such as the Fourier-Mellin and the complex moment and even the Zernike and the wavelet moment could substantially deviate from the actual value under the impact of the transformational noise. Therefore, the quality of features should not only be evaluated by sensitivity to high frequency noise but also to rotations and scaling. Our experiments show that invariant moments based on the appropriately chosen family of the wavelet radial functions are seemingly less affected by the transformational noise. Therefore, a system based on the rotation invariants should be subjected to a series of tests involving rotated and scaled images. The discriminative features should be selected from the less noise sensitive radial functions. Appropriately selected wavelets constitute the best choice for such a series of tests.

References

[1] S. Paschalakis, P. Lee, Pattern recognition in gray level images using moment based invariant features, Image Processing and its Applications, Conference Publication 465 (1999) 245–249.
[2] J. Shen, W. Shen, D. Shen, On Geometric and Orthogonal Moments, Multispectral Image Processing and Pattern Recognition, Series in Machine Perception Artificial Intelligence, 44, World Scientific, Singapore, 2001. 17–36.
[3] C.H. Teh, R.T. Chin, On image analysis by the methods of moments, IEEE Transactions on Pattern Analytical Machine Intelligence 10 (4) (1988) 496–512.

[4] R. Mukundan, K.R. Ramakrishnan, Fast computation of Legendre and Zernike moments, Pattern Recognition 28 (9) (1995) 1433–1442.
[5] S.X. Liao, M. Pawlak, Moment Invariants for Image Analysis with Applications to Image Reconstruction. Conference on Communication, power and Computing WESCANEX'97 IEEE Proceedings, Winnipeg, 1997, pp. 157–162.
[6] S.X. Liao, M. Pawlak, On the accuracy of Zernike moments for image analysis, IEEE Transactions on Pattern Analysis and Machine Intelligence 20 (12) (1998) 1358–1364.
[7] Y. Li, Reforming the theory of invariant moments for pattern recognition, Pattern Recognition 25 (1995) 115–123.
[8] C. Kan, M.D. Srinath, Invariant character recognition with Zernike and orthogonal Fourier-Mellin moments, Pattern Recognition 35 (2002) 143–154.
[9] J. Flusser, On the independence of rotation moment invariants, Pattern Recognition 33 (2000) 1405–1410.
[10] J. Flusser, On the inverse problem of rotation moment invariants, Pattern Recognition 35 (2002) 3015–3017.
[11] M.K. Yanni, The Influence of Thresholding and Spatial Resolution Variations on the Performance of the Complex Moment Descriptor Feature Extraction, PhD Thesis. The University of Kent, 1995.
[12] R. Mukundan, S.H. Ong, P.A. Lee, Image analysis by Tchebichef moments, IEEE Transactions on Image Processing 10 (9) (2001) 1357–1364.
[13] P. Yap, R. Paramesran, S. Ong, Image analysis by Krawtchouk moments, IEEE Transactions on Image Processing 12 (11) (2003) 1367–1377.
[14] D. Shen, H.H. Ip, Discriminative wavelet shape descriptors for recognition of 2-D patterns, Pattern Recognition 32 (1999) 151–165.
[15] C. Kan, M.D. Srinath, Combined Features of Cubic B-Spline Wavelet Moments and Zernike Moments for Invariant Character Recognition. Conference on Communication, Power and Computing, WESCANEX'01 IEEE Proceedings, 2001, pp. 511–515.
[16] M. Thuillard, Wavelets in Soft Computing, Wavelets in Soft Computing, Series in Robotices and Intelligent Systems, vol. 25, World Scientific, Singapore.
[17] J.A. Wickham Jr., Visual Aircraft Recognition, Manual of Headquarters Department of the Army, US Army Air Defense Artillery School, Washington DC, London, 1986.
[18] The Fine Arts Department of Thailand, Visual Database of Thai Musical Instruments, Manual of the Fine Arts Department, Wattanapanit Press, Bangkok, 2000.